2-2016

Evaluation of Nitrous Acid Sources and Sinks in Urban Outflow

Elliott T. Gall
Portland State University, gall@pdx.edu

Robert J. Griffin
Rice University

Allison L. Steiner
University of Michigan

Jack Dibb
University of New Hampshire, Durham

Eric Scheuer
University of New Hampshire

See next page for additional authors

Citation Details

Gall, E.T., Griffin, R.J., Steiner, A.L., Dibb, J., Scheuer, E., Gong, L., Rutter, A.P., Cevik, B.K., Kim, S., Lefer, B., Flynn, J., Evaluation of nitrous acid sources and sinks in urban outflow, Atmospheric Environment (2016).

Accepted Manuscript

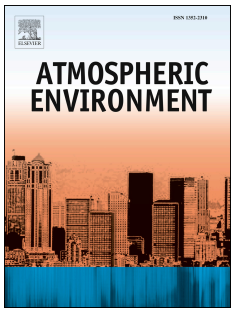

Evaluation of nitrous acid sources and sinks in urban outflow

Elliott T. Gall, Robert J. Griffin, Allison L. Steiner, Jack Dibb, Eric Scheuer, Longwen Gong, Andrew P. Rutter, Basak K. Cevik, Saewung Kim, Barry Lefer, James Flynn

PII: S1352-2310(15)30622-1

DOI: 10.1016/j.atmosenv.2015.12.044

Reference: AEA 14357

To appear in: *Atmospheric Environment*

Received Date: 24 April 2015

Revised Date: 15 December 2015

Accepted Date: 16 December 2015

Please cite this article as: Gall, E.T., Griffin, R.J., Steiner, A.L., Dibb, J., Scheuer, E., Gong, L., Rutter, A.P., Cevik, B.K., Kim, S., Lefer, B., Flynn, J., Evaluation of nitrous acid sources and sinks in urban outflow, *Atmospheric Environment* (2016), doi: 10.1016/j.atmosenv.2015.12.044.

Evaluation of nitrous acid sources and sinks in urban outflow

Elliott T. Gall[1,2,3], Robert J. Griffin[1*], Allison L. Steiner[4], Jack Dibb[5], Eric Scheuer[5], Longwen Gong[1,6], Andrew P. Rutter[1,7], Basak K. Cevik[1], Saewung Kim[8], Barry Lefer[9,10], James Flynn[9]

[1]Rice University, Department of Civil and Environmental Engineering, Houston, TX 77005
[2]Portland State University, Department of Mechanical and Materials Engineering, Portland, OR 97201
[3](Current) Nanyang Technological University & Berkeley Education Alliance for Research in Singapore, Singapore 138602
[4]University of Michigan, Department of Atmospheric, Ocean, and Space Sciences, Ann Arbor, MI 48109
[5]University of New Hampshire, Earth Systems Research Center, Durham, NH 03824
[6](Current) California Air Resources Board, Monitoring and Laboratory Division, Sacramento, CA 95811
[7] S.C. Johnson, Inc., Collaborative Sciences Division, Racine, WI 53403
[8]University of California – Irvine, Department of Earth System Science, Irvine, CA 92697
[9]University of Houston, Department of Earth and Atmospheric Sciences, Houston, TX 77004
[10] NASA Headquarters, Tropospheric Composition Program, Washington, DC 20546

[*]Corresponding author: Robert J. Griffin (rob.griffin@rice.edu)

ABSTRACT

Intensive air quality measurements made from June 22-25, 2011 in the outflow of the Dallas-Fort Worth (DFW) metropolitan area are used to evaluate nitrous acid (HONO) sources and sinks. A two-layer box model was developed to assess the ability of established and recently identified HONO sources and sinks to reproduce observations of HONO mixing ratios. A baseline model scenario includes sources and sinks established in the literature and is compared to scenarios including three recently identified sources: volatile organic compound-mediated conversion of nitric acid to HONO (S1), biotic emission from the ground (S2), and re-emission from a surface nitrite reservoir (S3). For all mechanisms, ranges of parametric values span lower- and upper-limit values. Model outcomes for 'likely' estimates of sources and sinks generally show under-prediction of HONO observations, implying the need to evaluate additional sources and variability in estimates of parameterizations, particularly during daylight hours. Monte Carlo simulation is applied to model scenarios constructed with sources S1-S3 added independently and in combination, generally showing improved model outcomes. Adding sources S2 and S3 (scenario S2/S3) appears to best replicate observed HONO, as determined by the model coefficient of determination and residual sum of squared errors ($r^2 = 0.55 \pm 0.03$, SSE = $4.6\times10^6 \pm 7.6\times10^5$ ppt^2). In scenario S2/S3, source S2 is shown to account for 25%and 6.7% of the nighttime and daytime budget, respectively, while source S3 accounts for 19% and 11% of the nighttime and daytime budget, respectively. However, despite improved model fit, there remains significant underestimation of daytime HONO; on average, a 0.15 ppt/s unknown daytime HONO source, or 67% of the total daytime source, is needed to bring scenario S2/S3 into agreement with observation. Estimates of 'best fit' parameterizations across lower to upper-limit values results in a moderate reduction of the unknown daytime source, from 0.15 to 0.10 ppt/s.

Keywords: air quality; unknown HONO source; Monte Carlo simulation; evolutionary solver

1. INTRODUCTION

Atmospheric nitrous acid (HONO) is important due to the role of HONO in generation of the hydroxyl radical (OH). There are a number of known sources of OH in the troposphere; however, OH production from HONO is of interest because the sources, fate, and diurnal cycling of HONO in the atmosphere have only recently begun to be elucidated. Models of atmospheric HONO generally employ a mass balance approach that allows evaluation of the HONO budget, often with a potentially limiting photostationary state assumption. As summarized by Spataro and Ianniello (2014) models generally include sources, sinks, and transport, the last relevant as formation processes hypothesized to occur at the ground result in vertical gradients of HONO.

Homogeneous and heterogeneous reactions, as well as direct emission of HONO from combustion sources, contribute to the presence of HONO in the troposphere (Finlayson-Pitts and Pitts, 1999). Nitrous acid strongly absorbs sunlight at wavelengths shorter than 390 nm resulting in photolytic degradation to OH and nitric oxide (NO). This results in suppressed, but non-zero, mixing ratios of daytime HONO due to the presence of daytime sources (Kleffmann, 2007). At night, the absence of this photolytic loss mechanism results in HONO accumulation, generally on the order of 0.1 ppb to 10 ppb (Kleffmann et al., 2003; Su et al., 2008; Young et al., 2012). The resumption of HONO photolysis after sunrise can lead to substantial formation of OH in the early morning. Alicke et al. (2003) report that during the BERLIOZ investigation at a rural, lightly trafficked site with low anthropogenic emissions during the summer months, photolysis of HONO was the dominant source of OH in the morning, and contributed as much as 20% of 24-h integrated OH production.

Modeling studies generally show the need for an unknown daytime source to close the HONO budget (Staffelbach et al., 1997; Lee et al., 2015). A number of photochemically driven

67 homogeneous reactions have been identified or considered: e.g., the known reaction of OH and
68 NO and the hypothesized reaction of photolytically excited nitrogen dioxide (NO_2) and water (Li
69 et al., 2008). The latter, however, may not proceed sufficiently rapidly or at adequate yields to
70 affect HONO mixing ratios in the atmosphere (Carr et al., 2009). Other potential homogeneous
71 sources are under discussion and review. For example, Li et al. (2014) proposed an internal
72 source of HONO that consumed nitrogen oxides, although follow up discussion and further
73 experiments indicate the source was likely strongly overestimated (Li et al., 2015; Ye et al.,
74 2015).

75 Nitrous acid formation mediated by aerosol surface area (SA) is a topic of ongoing
76 research, largely because the complexity of aerosols results in substantial uncertainty regarding
77 their ultimate role in HONO formation. Static surfaces such as the ground (Stemmler et al.,
78 2006) also may enhance HONO formation. Other hypothesized daytime sources include
79 emissions resulting from acid/base chemistry in soils (Su et al., 2011) and photolysis of nitric
80 acid (HNO_3) on forest canopy surfaces (Zhou et al., 2011). Photoenhanced conversion of NO_2 on
81 organic surfaces, including the ground and aerosols, are also thought to contribute to the daytime
82 HONO budget (George et al., 2005; Stemmler et al., 2006, 2007).

83 Given the many identified and proposed HONO source and sink mechanisms, single
84 value estimates of parameterizations of HONO sources and sinks limit the ability to understand
85 the impact of variability in multiple input parameters on models of HONO dynamics in the
86 atmosphere. Monte Carlo simulation (MCS) provides a tool to observe the combined effects of
87 ranges of input parameters and the resulting impact on the agreement between model output and
88 measurements. In this work, we identify fourteen HONO sources or sinks established in the
89 literature, including three sources that have recently (2013-2014) been identified. We evaluate

these recently identified sources through incorporation into a baseline model with a full-factorial, deterministic screening analysis. We then identify scenarios for which we stochastically parameterize source and sink mechanisms with MCS to determine probability distributions of modeled HONO mixing ratios.

2. METHODS

2.1 Measurements

Measurements of gas- and particle-phase constituents were made from May 30 to July 1, 2011 in a semi-urban area approximately 68 km northwest of the Dallas-Fort Worth (DFW) metropolitan area. The monitoring site was co-located with the Texas Commission on Environmental Quality Eagle Mountain Lake (EML) continuous ambient monitoring station (CAMS 75). Further details regarding the geography, surrounding industrial and biogenic activities, and site conditions have been outlined previously (Rutter et al., 2015)

Temperature, humidity (Vaisala, HMP-45C in a RM Young 10-plate solar radiation shield), and planetary boundary layer (PBL) height (Vaisala, CL31) were measured throughout the duration of the campaign. Mixing ratios of HONO and HNO_3 were measured every five minutes using a method that coupled a mist chamber with ion chromatography (Dionex, CD20-1), described in greater detail elsewhere (Dibb et al., 2004). First-order photolysis rate constants (*j*-values) were determined with radiometric measurements of actinic flux determined with a 2-pi double monochrometer with photomultiplier and subsequent calculations following IUPAC recommendations. Nitrogen oxides were recorded every minute using a chemiluminescence trace level NO-NO_2-NO_x analyzer (Thermo Electron Corp., Model 42C) equipped with a Blue Light Converter (Air Quality Design, Inc.) for NO_2 quantification. Hydroxyl radical was observed using atmospheric pressure chemical ionization mass spectrometry (Kim et al., 2013). One-hour

113 averaged mixing ratios of volatile organic compounds (VOCs) were measured using a thermal
114 desorption gas chromatograph with flame ionization detection (Perkin-Elmer O_3 Precursor
115 Analyzer System). Continuous measurements of number-based particle size distributions
116 (diameter range of 20 nm to 500 nm) were made every ten minutes with a scanning electrical
117 mobility sizer (SEMS, Brechtel Inc. Model 2002) and were converted to SA distributions
118 assuming spherical particles. Concentrations of particulate phase nitrate were determined with an
119 Aerodyne high-resolution time-of-flight aerosol mass spectrometer, as described by Rutter et al.
120 (2015). Black carbon concentrations were measured using an aethalometer.

121 *2.2 Baseline model*

122 A two-layer box model describing HONO mixing ratios was developed, with the height
123 of the first layer set to 36 m to represent a surface layer and the height of layer 2 set to 72 m to
124 facilitate use of HONO observations above the surface layer that are available in the literature.
125 Established source (labeled as 'B1-B8' in Table 1) and sink mechanisms (labeled 'L1-L3' in
126 Table 1) are described in full in the Supporting Information (SI) (including Figures S1-S5 and
127 equations S1-S20). The timeframe selected for continuous modeling was 22 June 01:00 to 25
128 June 14:00 (all times local) based on the longest uninterrupted period during the campaign with
129 observations of HNO_3, HONO, aerosol SA, NO_2, NO, gas-phase chloride (assumed to be
130 hydrochloric acid, HCl), and j_{HONO}. Mixing ratios of constituents during this period were
131 generally typical of the broader study period. Equation 1 describes baseline sources and sinks
132 modeled with a transient approach:

$$\frac{d[\mathrm{HONO}]_{trans}}{dt} = F_{B1} + F_{B2} + F_{B3} + F_{B5} + F_{B6} + F_{B7} + F_{B8} - \left(F_{L1} + F_{L2} + F_{L3}\right) - \Psi_{trans} \quad (1)$$

where $[HONO]_{trans}$ is the mixing ratio of HONO from modeled transient sources and sinks (ppt), *dt* is the time step (s) between measurements for which observations of all constituents present in Equation 1 were made, *F* represents the source or sink strength of the indicated mechanism (ppt/s), and Ψ_{trans} is the loss (or source) of HONO from layer 1 to (or from) layer 2 due to vertical transport (ppt/s).

Equation 1 describes the transient processes occurring in the model; source B4 was incorporated into the model after accounting for transient processes as shown in Equation 2:

$$[\mathrm{HONO}]_{\mathrm{total}} = [\mathrm{HONO}]_{\mathrm{trans}} + f_{\mathrm{emiss}}\Delta[\mathrm{NO_x}] \quad (2)$$

where $[HONO]_{total}$ is the mixing ratio of HONO at a time step resulting from transient and instantaneous processes (ppt) and f_{emiss} is the direct HONO emission factor described in Table 1. Equation 2 may overestimate the contribution of B4 in a box-model, as during the daytime, HONO will rapidly photolyze prior to the measurement of emitted NO_x.

Vertical transport, Ψ_{trans} (ppt/s), is calculated using a first-order flux-gradient relationship simulated with the 1D CACHE model (Bryan et al., 2012) where mass is transported by eddy diffusion at a magnitude proportional to the eddy diffusivity for heat (K_h), shown in equation 3:

$$\Psi_{trans} = -K_h(z,t)\frac{\partial C(z,t)}{\partial z}\frac{1}{h} \quad (3)$$

where $K_h(z,t)$ is the eddy diffusivity (m^2/s) at height *z* (m) and time *t.* As shown in equation 3, estimates of flux are divided by *h*, the height of the second layer in the model (m), prior to inclusion in equation 1.

Two 1D simulations during the campaign were used to derive K_h, including one simulation for 7-9 June and one for 10-12 June. For the layers corresponding to the upper boundary that are used in the results here, K_h is derived based on a length scale, vertical wind

153 shear, and a stability parameter (Forkel et al., 1990). It is calculated at each time step within the
154 model, providing a diurnal cycle that is based on meteorological conditions during the campaign.
155 Observations of HONO were made at one elevation, approximately 10 m above surface,
156 and were used to represent the HONO mixing ratio in layer 1 of the model. Equation 3 requires
157 an estimate of the HONO mixing ratio in layer 2 to estimate the HONO gradient. Three scenarios
158 were considered: 1) no gradient (i.e., [HONO] in layer 1 equals that in layer 2 at all times); 2) a
159 gradient created using fractions of [HONO] presented in Vandenboer et al. (2013), representative
160 of a stronger nighttime gradient and a weaker daytime gradient (GrN); and 3) a gradient created
161 from fractions of [HONO] presented in Villena et al. (2011) that is representative of a stronger
162 daytime gradient and weaker nighttime gradient (GrD). Diurnal profiles of the three gradient
163 conditions are shown in Figure S6 of the SI and implications of this limitation are discussed in
164 Section 3.2.

165 *2.3 Parameterization and evaluation of newly identified HONO sources*

166 Three recently identified HONO source mechanisms were parameterized to assess the
167 potential of these mechanisms (in conjunction with B1-B8 and L1-L3) to independently or
168 jointly account for HONO mixing ratios observed in DFW. The three mechanisms, listed in
169 Table 1 as S1, S2, S3 are incorporated into Equation 1 as additional sources of HONO.

170 Source S1 is the formation of HONO from the reduction of HNO_3 to HONO mediated by
171 VOCs emitted from motor vehicles (Rutter et al., 2014). The source strength (F_{S1}, ppt/s) was
172 parameterized using HONO source strength and reactant mixing ratios presented in Table 1 of
173 Rutter et al. (2014) and is shown in equation 4:

$$F_{S1} = f_{HNO_3,VOC}\left[\frac{\left(\frac{[\text{Propylene}]}{[\text{Benzene}]}\right)_{EML}}{\left(\frac{[\text{Propylene}]}{[\text{Benzene}]}\right)_{Max,DFW}}\right]\left[\frac{[\text{HNO}_3]_{\text{EML}}}{[\text{HNO}_3]_{\text{rutter}}}\right] \quad (4)$$

where $f_{HNO3,VOC}$ is the observed HONO formation rate (ppt s^{-1}) in Rutter et al. (2014), and normalizing ratios are further described in the SI. Estimates of 'likely' $f_{HNO3,VOC}$ were taken for experiments conducted at 50% RH while 'lower-limit' and 'upper-limit' estimates were taken as the minimum and average across experiments shown in Table 1 of Rutter et al. (2014). Normalizing assumptions shown in equation 4 resulted in, on average, ~95% reduction of $f_{HNO3,VOC}$ when calculating $F_{S1.}$ The form of the parameterization in equation 4 is speculative; propylene is chosen as a proxy for reactive VOCs while benzene is chosen to account for dilution that may occur as air masses move from DFW to EML (see Figure S7 in the SI for a diurnal profile of propylene/benzene). Identification of specific reactive species participating in the HONO formation process identified in Rutter et al. (2014) would enable improvements in development and assessment of parameterizations of VOC-mediated conversion of HNO_3 to HONO.

Source S2 is HONO emissions from soil bacteria as described by Oswald et al. (2013). Emission from the soil (F_{S2}, ppt/s) was assumed to mix instantaneously through the first model layer as shown in equation 5:

$$F_{S2} = \frac{f_{soil}}{h}\Gamma_{S2} \quad (5)$$

where f_{soil} is the "optimum" HONO flux from a soil type (molec cm^{-2} s^{-1}), h is the height of the model layer, and Γ_{S2} represents the conversion factor to ppt/s prior to inclusion in equation 1 (see the SI equations S21-S24 for an example calculation). The 'lower-limit' value of f_{soil} was taken

as the value of HONO flux for pasture, and the 'upper-limit' value was taken as that for grassland. No 'likely' value of f_{soil} was selected, as pasture and grassland were the only two relevant soil types for the DFW region. Despite specifying a 'lower-limit' value, this investigation may be effectively considering the high end of contribution of soil bacteria to HONO because "optimum" values of flux are used for both soil types.

Source S3 is the re-emission of HONO from a surface nitrite reservoir by displacement from HNO_3 and HCl, as in Vandenboer et al. (2014, 2015) and shown in equation 6:

$$F_{S3} = \frac{[HNO_3] + [HCl]}{h} v_d \eta \quad (6)$$

where F_{S3} is the source strength of S3 (ppt s^{-1}), v_d is the deposition velocity of HNO_3 and HCl, taken as 1 cm s^{-1}, and η is the displacement efficiency, ranging from 1% to 9% to 20% for 'lower-limit', 'likely', and 'upper-limit' values, respectively (VandenBoer et al., 2014). This parameterization was constrained by the calculation of a 'reservoir' of nitrite from deposited HONO, approximated from a material balance on the ground where the source of nitrite is mechanism L1 and loss is due to displacement from mechanism S3. Mechanism S3 was set to 0 when the reservoir was equal to 0. As there may be additional sources of surface nitrite other than gas-phase HONO and surface nitrite accumulation over greater than diurnal time-scales, equation 6 likely represents a conservative estimate of the source strength of S3. Further description of the constraints on source S3 is given in the SI and dynamics are depicted in Figure S8, also in the SI.

2.4 Model calculation and assessment

Nitrous acid mixing ratios were first modeled with the baseline scenario using the B and L parameterizations summarized in Table 1. The 'likely' parameterization incorporates HONO

source and sink estimations thought most representative of each mechanism, while 'upper-limit' and 'lower-limit' are values that result in maximum or minimum HONO production, respectively, e.g. in the 'upper-limit', parameterizations of sources result in greater formation while those of sinks result in lower loss rates. Predictions of HONO mixing ratios were assessed through the residual sum of squared errors (SSE) and the coefficient of determination (r^2), both determined from differences between modeled and measured HONO mixing ratios.

Model scenarios were constructed to assess the three new mechanisms (mechanism ID = S1, S2, and S3 shown in Table 1) and gradient conditions (GrN or GrD); scenarios are named according to the gradient used and sources added, e.g., GrN S2/S3 refers to a model scenario with the stronger nighttime gradient as described previously and with sources S2 and S3 added to baseline sources B1-B8 and sinks L1-L3. Sources S1-S3 were added to the baseline model in a full-factorial deterministic screening analysis (using 'likely' estimates of parameterizations) to identify scenarios for further analysis. Monte Carlo simulation (Crystal Ball v. 11.1.2.3, Oracle) was used to evaluate the probability of model scenarios to account for observed HONO mixing ratios. Input distributions of source and sink parameterizations were assumed to be triangular probability distributions, bounded by 'lower-limit' and 'upper-limit' values with the 'likely' value as the most frequently occurring. Model sensitivity to the number of trial simulations was performed to ensure a trial-independent solution was achieved; all MCS were conducted with 5,000 iterations. A bounded evolutionary solver was applied to the baseline model scenario and to the model scenario with the highest r^2 and lowest residual SSE in the deterministic screening analysis. The evolutionary solver used a genetic algorithm to estimate source and sink parameterizations with a minimum SSE across the range of 'lower-limit' to 'upper-limit' values for each source or sink mechanism.

3. RESULTS AND DISCUSSION

3.1 Ambient air monitoring in the outflow of DFW

Experimental observations of mixing ratios of ambient gases and particles input to the model are shown in Figure 1; diurnal profiles of selected constituents across the full monitoring campaign are shown in Figure S9 of the SI. Values of $HONO/NO_2$ are variable and elevated during the daytime, possibly indicative of a secondary daytime source of HONO. Mixing ratios of HNO_3 are suppressed in the morning and evenings and elevated during daytime hours, likely a result of strong daytime HNO_3 production from the reaction of NO_2 and OH (Aneja et al., 1994). The highest observed mixing ratios of HNO_3 across the full monitoring campaign are included in the model period shown in Figure 1, exceeding 5000 ppt in the early evening of June 22, 2011. Mixing ratios of HCl exhibit similar trends to those observed for HNO_3. Mixing ratios of HONO show accumulation over the nighttime and suppression during the daytime, a result of the strong loss due to photolysis and convective dilution during the daytime hours. Aerosols and aerosol-phase constituents appear elevated during the nighttime hours of 6/23 and 6/24 compared to daytime concentrations, but are suppressed during the nighttime of 6/25. Across the model period, the SA of particulate matter averages 125 $\mu m^2\ cm^{-3}$, consistent with typical values across the month-long monitoring campaign (Figure S1), and ranges 22 $\mu m^2\ cm^{-3}$ - 392 $\mu m^2\ cm^{-3}$.

3.2 Baseline model

Mixing ratios of HONO are first calculated with the model under the baseline scenario for 'likely' estimates of parameterizations. Predicted and measured mixing ratios of HONO for the baseline scenario with three HONO gradient conditions described in Section 2.2 are shown in Figure 2. The "no gradient" condition results in substantial over-estimation of nighttime HONO mixing ratios, logical given the role of the ground surface in HONO formation processes

included in the baseline scenario and the first layer height of 36 m. Conversely, the GrN and GrD conditions both result in underestimation of nighttime HONO, with relatively small differences between the two conditions. A strong daytime sink, due to photolysis, results in suppression of modeled daytime mixing ratios below observation for all three gradient conditions, implying the need for daytime sources beyond those considered in the baseline scenario. The underestimation may also result from the limited vertical resolution in the two-layer box model used here and the measurement height in the lower portion of the first layer (10 m); it is likely that a continuous HONO gradient is present in the 36 m of the model first layer resulting in a lower modeled mixing ratio across the first model layer than the 10 m observation.

While relatively few studies report measurements of vertical gradients of HONO, available profiles generally show higher HONO mixing ratios in surface layers than aloft, indicative of ground surface HONO formation. Michoud et al. (2014) summarize several studies reporting vertical gradients, four of which show the presence of a vertical gradient (Veitel, 2002; Zhang et al., 2009; Villena et al., 2011; Wong et al., 2012) and one that does not (Häseler et al., 2009). Vandenboer et al. (2013) report high-resolution vertical profiles measured from a tower in Boulder, CO, and show the presence of both daytime and nighttime HONO gradients. Veitel et al. (2002) report that over 13 months of measurements, HONO mixing ratios were observed to decrease with height under nearly all atmospheric conditions. For the present investigation, we interpret the over-prediction of HONO mixing ratios in the nighttime for the “no gradient” condition, when convective mixing is most likely to be diminished, to indicate a HONO vertical gradient. Thus, conditions GrN or GrD better represent the vertical structure of HONO mixing ratios in the outflow of DFW. While this appears to be in agreement with the preponderance of available HONO vertical gradient measurements, a site-specific HONO gradient would clearly

improve the present study. Nevertheless, parameterizations here allow an estimation of the source and sink processes in the outflow of DFW and exploration of two estimates of gradients to assess model sensitivity to the HONO vertical profile. The impact of the vertical gradient and of parameterizations of established and recently identified HONO sources and sinks are further explored in Sections 3.3-3.5.

3.3 Deterministic screening analysis

A deterministic screening analysis was employed to evaluate model outcomes when sources S1-S3, acting independently or in any combination, are incorporated into the model. This full-factorial analysis, consisting of 24 possible scenarios, is conducted for only the 'likely' parameterizations of the mechanisms, as shown in Table S1 of the SI. Full output of model runs across all gradient conditions and scenarios of parameterizations are provided in Figures S10-S12.

Generally, 'likely' estimates of parameterizations showed improved model fit compared to 'upper-limit' estimates, implying additional sources of HONO, rather than increased production from baseline sources result in improved model outcomes. Subsequent discussion in this section reflects 'likely' parameterizations. Scenarios identified for further investigation are those with a combination of low SSE and high r^2. The baseline model generally is characterized by the highest model SSE, and the addition of source mechanisms S1-S3 generally lowers SSE and increases r^2. In cases, however, the SSE is lowered while the r^2 decreases (for example, from GrN Baseline to GrN S1). This is a result of improvement in model prediction for only a subset of times in the modeling period. The screening analysis identified scenario S2/S3 and scenario S1/S2/S3 as having the lowest SSE and highest r^2 (SSE range: 4.3×10^6–6.7×10^6; r^2 range: 0.42-

304 0.58). These scenarios, along with baseline scenarios for comparison, are further explored with
305 MCS and an evolutionary solver.

306 *3.4 Monte Carlo simulation*

307 Six model scenarios that vary the new sources and vertical gradient conditions were
308 evaluated with MCS to incorporate uncertainty and variability in each mechanism into the
309 model; model estimates of HONO are determined as probabilistic distributions at each model
310 time step. Summarized output of MCS are shown in Figure 3 as hourly-averaged diurnal profiles
311 of measured and modeled distributions of HONO mixing ratios across the model period. The
312 MCS reinforces the conclusions that 'baseline' source mechanisms cannot explain observed
313 HONO mixing ratios; in the GrN Baseline condition, 90^{th} percentile values of model output
314 underestimate observed HONO mixing ratios in 23 of 24 reported hours, and 75^{th} percentile
315 values underestimate observed HONO mixing ratios all 24 reported hours.

316 The addition of source mechanisms S2 and S3 to the model (Figure 3) results in
317 improved agreement between the model and observations for nighttime mixing ratios of HONO
318 for both GrN and GrD conditions. GrN S2/S3 shows 9 of the 10 hours in the 21:00-07:00
319 nighttime period are between the 10^{th} and 90^{th} percentile values determined in the model. GrD
320 S2/S3 shows improvement over the GrD Baseline condition; however, metrics of goodness of fit
321 are lower than GrN S2/S3, and there is less improvement over baseline. This appears to be a
322 result of sustained accumulation over the nighttime period, due to the smaller HONO nighttime
323 vertical gradient in the GrD condition. Under both GrN and GrD conditions for scenario S2/S3,
324 daytime mixing ratios of HONO remain substantially underpredicted as in the baseline condition.

The addition of all three sources (S1, S2, and S3) does not appear to resolve underprediction of the daytime HONO mixing ratio. In the GrN condition, the addition of source S1 results in a small increase in over-estimation of nighttime HONO mixing ratios and metrics of model fit worsen. In the GrD condition, there is a limited impact from the combined effect of sources S1, S2 and S3, with a modest reduction in both SSE and correlation coefficient when comparing GrD S1/S2 to GrD S1/S2/S3. Figure 3 shows GrN S2/S3 results in improved model fit compared to other scenarios, although daytime HONO remains substantially underestimated.

An estimation of average total and relative source and sink strength across both nighttime (21:00 – 07:00) and daytime (07:00 – 21:00) is shown in Figure 4 for GrN S2/S3. Estimates of sources and sinks are reported for 'likely' values of parameterizations for the indicated time period. Considerable temporal differences in the contributions of various source and sinks to the HONO budget exist. At night, HONO from NO_2 conversion at the ground (B7) is the major source, contributing 53% of the HONO budget. Biotic release from the ground (S2) and re-emission from the nitrite reservoir (S3) are the next two largest contributors at 25% and 19%, respectively. Nighttime HONO is slightly over-estimated; an 'unknown' nighttime sink of 0.0016 ppt/s, or 3% of the total, is required to bring the model into agreement with observations. Major nighttime sinks are vertical transport and deposition of HONO at the ground surface, contributing 73% and 21%, respectively. These nighttime sources and sinks are in general agreement with relative estimates of mechanisms reported by Czader et al. (2012), who report 71% of HONO production due to heterogeneous surface chemistry and losses due to transport and deposition of 77% and 23%, respectively, during the nighttime and pre-sunrise morning.

During the daytime, a missing HONO source dominates; however there are meaningful contributions to the daytime HONO budget from S3, S2, B8, B7 and B5. A missing daytime

source of 0.15 ppt s^{-1}, or 67% of the total HONO source budget shown in Figure 4, is needed to bring modeled and measured results into full agreement. This "missing" source is in the range of magnitudes identified in other investigations, ranging from 0.03 - 0.3 ppt s^{-1} (Su et al., 2008; Elshorbany et al., 2009; Sörgel et al., 2011; VandenBoer et al., 2013; Lee et al., 2015). Unless there is a positive artifact that depends on sunlight, a strong daytime source is needed to balance the substantial sink of HONO due to photolysis (89% of the total sink). In section 3.5, we explore the potential for 'best fit' estimates of parameterizations in GrN S2/S3 to close some portion of the HONO budget through optimization of parameterizations across the range of values presented in Table 1.

3.5 Evolutionary solver and sensitivity analysis

An evolutionary solver was employed to estimate the optimal combination of input values within 'lower-limit' to 'upper-limit' ranges of parameterizations and the resulting impact on the estimate of the "missing" HONO source or sink. The evolutionary solver was applied to the GrN baseline scenario and GrN S2/S3. Model outcomes with optimal estimates for GrN baseline and GrN S2/S3 are shown in Figure 5 and parameterizations are reported in Table 2.

Across optimization of both GrN Baseline and GrN S2/S3, the largest changes to the parameterizations relate to heterogeneous conversion of NO_2 on aerosol (B1 and B2) and on the ground (B7, B8), and HONO uptake to the ground (L1). Aerosol processes increase substantially as a result of a speculative upper-limit as described in the SI; B1 was allowed to vary over 1.5 orders of magnitude and B2 over 2.5 orders of magnitude based on prior modeling studies, rather than experimental estimates. However, contributions from B1 and B2 remain limited (< 1% as can be determined from absence of B1 and B2 in Figure 4), in part a result of the two layer box-model used here that emphasizes ground-level phenomena. In both GrN Baseline and GrN

S2/S3, the optimization resulted in B8 at the upper-limit of the parameterization. Source B7 increased by ~2× in GrN Baseline, but more moderately in GrN S2/S3, a result of the contribution of sources S2 and S3 in GrN S2/S3. In GrN S2/S3, deposition loss (L1) increased, a result of the need to balance increases in parameterizations of sources that act over both daytime and nighttime periods (e.g., S3) and contribute to reductions in the daytime "unknown" source but also nighttime accumulation.

Figure 5 shows greater improvements in metrics of model goodness of fit for the optimal solution of GrN S2/S3 compared to the optimal solutions of the GrN Baseline. This indicates that baseline mechanisms are not able to similarly explain HONO observations under any combination of input parameters compared to the scenario with S2/S3 present. This appears to largely result from stronger parameterizations of S2/S3 resulting in improved estimates of daytime HONO mixing ratio, although levels are still lower than observed. Best-fit parameterizations of GrN S2/S3 result in a missing daytime source of 0.10 ppt/s, reduced from 0.15 ppt/s (Figure 4), implying that a substantial missing HONO source remains even across a statistically optimized range of parameterizations.

The "best-fit" estimates of GrN S2/S3 reflect an improved statistical outcome for the model when parameterizations are allowed to vary across a range of values. Parameterizations in Table 2 with larger percentage changes imply a combination of model sensitivity to the parameter as well as uncertainty in the value of the parameterization. We conducted a sensitivity analysis to identify the most important parametrizations impacting the estimates of goodness-of-fit, the model r^2 and SSE. The sensitivity analysis for GrN S2/S3 is summarized in Table S2 of the SI, reported as the Spearman's rank correlation coefficient (ρ) between each mechanism's input parameter and the model output r^2 or SSE. Uptake of NO_2 at the ground (B7) is the

parameter with the largest impact on both the model SSE and r^2, by a comparatively large margin. Given that there is a wide range of estimates of the uptake coefficient parameterizing B7 in the literature, this source represents a large source of uncertainty in the model. Sources S3, B8, and S2 are the next three strongest correlations with model SSE; interestingly, all four sources with highest sensitivity (B7, B8, S2, and S3) are ground-level phenomena. Source B7 was strongest correlated with night-time (21:00-07:00) HONO mixing ratios while source S3 was strongest correlated with daytime HONO. This underscores the importance of characterizing the role of the ground surface mechanisms, including biotic release and ground-level chemical transformations.

The presence of a substantial missing daytime source is further explored via estimation of correlation coefficients between measured constituents and products of constituents with the missing HONO source, similar to the analysis presented by Lee et al. (2015). This analysis employed time-series measurements for constituents and the estimate of missing HONO at each time step required for model agreement with observation. Outcomes are shown in Table S3 for 'likely' and 'best-fit' estimates of GrN S2/S3. Relatively strong correlation coefficients ($r^2 > 0.5$) were observed for j_{NO2} and j_{NO2} × temperature with the missing HONO source, the latter in close agreement to the results of Lee et al (2015). However, the correlation of $j_{NO2} \times NO_2$ with the missing HONO source is weak ($r^2 = 0.09 - 0.17$), as is the correlation of j_{NO2} × SEMS SA× NO_2 ($r^2 = 0.08 - 0.16$) and with NO_2 alone ($r^2 = 0.21$-0.25). The stronger correlation with j_{NO2} and j_{NO2} × temperature may imply photosensitized conversion on organics, including humic acids, which are mainly ground surface sources (Stemmler et al., 2006, 2007), are underestimated. The weak correlation of the missing HONO source with NO_2 and products containing NO_2 mixing ratios appears aligned with a recent analysis of weekday-weekend HONO and NO_2 relationships

that shows HONO production rates do not increase with increases in NO_2, implying daytime HONO production may not be rate-limited by NO_2 (Pusede et al., 2015). Weakening correlations for products of gas- and particle-phase constituents and j_{NO2} also may result from the two-layer model that lends greater emphasis to interactions at the ground level, consistent with the results of the sensitivity analysis in Table S2 and discussed previously.

3.6 Model limitations

The model described in this work is subject to a number of important limitations. Source S1 assumes the source strength determined in the laboratory is possible in the ambient environment, with several normalizing assumptions. However, as we did not observe meaningful formation of HONO from source S1, the impact of the speculative parameterization is therefore limited in this investigation. Future field efforts should further investigate the potential for VOC-mediated reduction of HNO_3 to HONO in near-source environments. Source S2 was parameterized using a single value for a model simulation; there are likely to be diurnal variations in biological activity and soil water content that would impact the parameterization of source S2. Source S3 considered only gas-phase HONO as an input to the surface nitrite reservoir and that the reservoir was empty at the beginning of the model period. This may result in a conservative estimate of the contribution of source S3.

Input distributions in MCS were assumed to be triangular. This assumption may over-weight estimates of parameterizations at the 'upper-limit' and 'lower-limit' extents of the distribution as compared to a normal distribution. A triangular distribution was chosen, in part, to ensure parameterizations did not exceed upper or lower-limit estimates in MCS. The two-layer box model uses instantaneous and *in-situ* mixing ratios to constrain the model, with the assumption of instantaneous mixing up to the first layer height. Transport between layers was

estimated using an approximation of HONO vertical gradients at similar heights taken from literature. We assume transport time for NO_x sources that exceeds the atmospheric age of HONO (Lee et al. 2013). During the daytime periods (07:00-21:00), the atmospheric age of HONO across the modeling period in this work averaged 19.4 min and ranged from 8.9 to 128 min. We assume NO_x sources input to the model originate from the metropolitan DFW area (~70 km away), while the wind speed averaged 19 km/h, resulting in a transport time of 220 min.

4. CONCLUSIONS

Model predictions of HONO that account for ranges in parameterizations of HONO source and sink mechanisms enable a statistical assessment of the likelihood of the model to match observation. Observations of HONO appear most accurately simulated when emission from soil biota (S2) and re-emission from a ground level nitrite source (S3) are included in the model. Model output for GrN S2/S3 accounted for, on average, 33% of the daytime HONO budget and 103% of the nighttime HONO budget. Major nighttime sources included (in order) NO_2 conversion at the ground (B7), biotic release from soil (S2), and re-emission from the nitrite reservoir (S3). Major daytime sources include S3, S2, photoenhanced NO_2 conversion at the ground (B8), B7, and the reaction of OH with NO (B5). Model fit improved after application of an evolutionary solver, resulting in a reduction of the estimate of the unknown daytime source for GrN S2/S3. However, the presence of a substantial unknown daytime source (on average 0.10 ppt/s) even with a statistically optimal fit for GrN S2/S3 implies additional sources of HONO than those evaluated here must be included to reproduce accurately daytime HONO mixing ratios. Analyses of model sensitivity and correlations between the missing HONO source and constituents imply the presence of additional, or underestimation of considered, ground-level HONO sources in this investigation.

ACKNOWLEDGEMENTS

The support of the Texas Commission on Environmental Quality Air Quality Research Program is gratefully acknowledged. We also thank the two reviewers whose comments and suggestions greatly improved the model and manuscript.

REFERENCES

Alicke, B., Geyer, A., Hofzumahaus, A., Holland, F., Konrad, S., Pätz, H-W. et al.. OH formation by HONO photolysis during the BERLIOZ experiment. J. Geophys. Res. Atmos. 108 (D4), 8247.

Aneja, V.P., Claiborn, C.S., Li, Z., Murthy, A., 1994. Trends, seasonal variations, and analysis of high-elevation surface nitric acid, ozone, and hydrogen peroxide. Atmospheric Environment 28, 1781–1790.

Aumont, B., Chervier, F., Laval, S., 2003. Contribution of HONO sources to the NOx/HOx/O3 chemistry in the polluted boundary layer. Atmospheric Environment 37, 487–498.

Bryan, A.M., Bertman, S.B., Carroll, M.A., Dusanter, S., Edwards, G.D., Forkel, R. et al., 2012. In-canopy gas-phase chemistry during CABINEX 2009: sensitivity of a 1-D canopy model to vertical mixing and isoprene chemistry. Atmos. Chem. Phys. 12, 8829–8849.

Carr, S., Heard, D.E., Blitz, M.A., 2009. Comment on "Atmospheric Hydroxyl Radical Production from Electronically Excited NO2 and H2O." Science 324, 336b.

Dibb, J.E., Scheuer, E., Whitlow, S.I., Vozella, M., Williams, E., Lerner, B.M., 2004. Ship-based nitric acid measurements in the Gulf of Maine during New England Air Quality Study 2002. J. Geophys. Res. Atmos. 109, D20303.

Elshorbany, Y.F., Kurtenbach, R., Wiesen, P., Lissi, E., Rubio, M., Villena, G. et al., 2009. Oxidation capacity of the city air of Santiago, Chile. Atmospheric Chemistry and Physics 9, 2257–2273.

Finlayson-Pitts, B.J., Pitts, J., 1999. Chemistry of the upper and lower atmosphere: Theory, experiments, and applications. Academic Press.

Forkel, R., Seidl, W., Dlugi, R., Deigele, E., 1990. A one-dimensional numerical model to simulate formation and balance of sulfate during radiation fog events. J. Geophys. Res. 95, 18501–18515.

George, C., Strekowski, R.S., Kleffmann, J., Stemmler, K., Ammann, M., 2005. Photoenhanced uptake of gaseous NO_2 on solid organic compounds: a photochemical source of HONO? Faraday Discuss. 130, 195–210; discussion 241–264, 519–524.

Häseler, R., Brauers, T., Holland, F., Wahner, A., 2009. Development and application of a new mobile LOPAP instrument for the measurement of HONO altitude profiles in the planetary boundary layer. Atmos. Meas. Tech. Discuss. 2, 2027–2054.

Kim, S., Wolfe, G.M., Mauldin, L., Cantrell, C., Guenther, A., Karl, T. et al., 2013. Evaluation of HOx sources and cycling using measurement-constrained model calculations in a 2-methyl-3-butene-2-ol (MBO) and monoterpene (MT) dominated ecosystem. Atmos. Chem. Phys. 13, 2031–2044.

Kirchstetter, T.W., Harley, R.A., Littlejohn, D., 1996. Measurement of nitrous acid in motor vehicle exhaust. Environ. Sci. Technol.30, 2843–2849.

Kleffmann, J., 2007. Daytime sources of nitrous acid (HONO) in the atmospheric boundary layer. Chemphyschem 8, 1137–1144.

Kleffmann, J., Becker, K.H., Wiesen, P., 1998. Heterogeneous NO_2 conversion processes on acid surfaces: possible atmospheric implications. Atmospheric Environment 32, 2721–2729.

Kleffmann, J., Kurtenbach, R., Lörzer, J., Wiesen, P., Kalthoff, N. et al., 2003. Measured and simulated vertical profiles of nitrous acid—Part I: Field measurements. Atmospheric Environment 37, 2949–2955.

Kurtenbach, R., Becker, K.H., Gomes, J.A.G., Kleffmann, J., Lörzer, J.C., Spittler, M. et al., 2001. Investigations of emissions and heterogeneous formation of HONO in a road traffic tunnel. Atmospheric Environment 35, 3385–3394.

Lee, J.D., Whalley, L.K., Heard, D.E., Stone, D., Dunmore, R.E., Hamilton, J.F., Young, D.E., Allan, J.D., Laufs, S., Kleffmann, J., 2015. Detailed budget analysis of HONO in central London reveals a missing daytime source. Atmos. Chem. Phys. Discuss. 15, 22097–22139.

Lee, B.H., Wood, E.C., Herndon, S.C., Lefer, B.L., Luke, W.T., Brune, W.H. et al., 2013. Urban measurements of atmospheric nitrous acid: A caveat on the interpretation of the HONO photostationary state. J. Geophys. Res. Atmos. 118, 12274-12281.

Li, S., Matthews, J., Sinha, A., 2008. Atmospheric hydroxyl radical production from electronically excited NO2 and H2O. Science 319, 1657–1660.

Li, X., Rohrer, F., Hofzumahaus, A., Brauers, T., Häseler, R., Bohn, B. et al., 2014. Missing Gas-Phase Source of HONO Inferred from Zeppelin Measurements in the Troposphere. Science 344, 292–296.

Li, X., Rohrer, F., Hofzumahaus, A., Brauers, T., Häseler, R., Bohn, B. et al., 2015. Response to Comment on "Missing gas-phase source of HONO inferred from Zeppelin measurements in the troposphere." Science 348, 1326e.

Michoud, V., Colomb, A., Borbon, A., Miet, K., Beekmann, M., Camredon, M., et al. 2014. Study of the unknown HONO daytime source at a European suburban site during the MEGAPOLI summer and winter field campaigns. Atmos. Chem. Phys. 14, 2805–2822.

Monge, M.E., D'Anna, B., Mazri, L., Giroir-Fendler, A., Ammann, M., Donaldson, D.J., George, C., 2010. Light changes the atmospheric reactivity of soot. PNAS 107, 6605–6609.

NASA, 2011. Chemical Kinetics and Photochemical Data for Use in Atmospheric Studies (No. JPL 10-6). California Institute of Technology, Pasadena, CA, Jet Propulsion Laboratory.

Oswald, R., Behrendt, T., Ermel, M., Wu, D., Su, H., Cheng, Y. et al., 2013. HONO emissions from soil bacteria as a major source of atmospheric reactive nitrogen. Science 341, 1233–1235.

Pusede, S.E., VandenBoer, T.C., Murphy, J.G., Markovic, M.Z., Young, C.J., Veres, P.R. et al., 2015. An Atmospheric Constraint on the NO_2 Dependence of Daytime Near-Surface Nitrous Acid (HONO). Environ. Sci. Technol. doi:10.1021/acs.est.5b02511

Rutter, A.P., Griffin, R.J., Cevik, B.K., Shakya, K.M., Gong, L., Kim, S., Flynn, J.H., Lefer, B.L., 2015. Sources of air pollution in a region of oil and gas exploration downwind of a large city. Atmospheric Environment. 120, 89–99.

Rutter, A.P., Malloy, Q.G.J., Leong, Y.J., Gutierrez, C.V., Calzada, M., Scheuer, E., Dibb, J.E., Griffin, R.J., 2014. The reduction of HNO3 by volatile organic compounds emitted by motor vehicles. Atmospheric Environment 87, 200–206.

Sörgel, M., Regelin, E., Bozem, H., Diesch, J.-M., Drewnick, F., Fischer, H. et al., 2011. Quantification of the unknown HONO daytime source and its relation to NO_2. Atmospheric Chem. Phys. 11, 10433–10447.

Spataro, F., Ianniello, A., 2014. Sources of atmospheric nitrous acid: State of the science, current research needs, and future prospects. J. Air Waste Manage. Assoc. 64, 1232–1250.

Staffelbach, T., Neftel, A., Horowitz, L.W., 1997. Photochemical oxidant formation over southern Switzerland, 2. Model results. Journal of Geophysical Research 102, 23363-23373.

Stemmler, K., Ammann, M., Donders, C., Kleffmann, J., George, C., 2006. Photosensitized reduction of nitrogen dioxide on humic acid as a source of nitrous acid. Nature 440, 195–198.

Stemmler, K., Ndour, M., Elshorbany, Y., Kleffmann, J., D'Anna, B., George, C.,et al., 2007. Light induced conversion of nitrogen dioxide into nitrous acid on submicron humic acid aerosol. Atmospheric Chem. Phys. 7, 4237–4248.

Su, H., Cheng, Y.F., Cheng, P., Zhang, Y.H., Dong, S., Zeng, L.M. et al, 2008. Observation of nighttime nitrous acid (HONO) formation at a non-urban site during PRIDE-PRD2004 in China. Atmospheric Environment 42, 6219–6232.

Su, H., Cheng, Y., Oswald, R., Behrendt, T., Trebs, I., Meixner, F.X., et al., 2011. Soil nitrite as a source of atmospheric HONO and OH radicals. Science 333, 1616–1618.

Trick, S., 2004. Formation of Nitrous Acid on Urban Surfaces - A physical-chemical Perspective. Dissertation. Universität Heidelberg, 2004, http://www.ub.uni-heidelberg.de/archiv/ 4814.

VandenBoer, T.C., Brown, S.S., Murphy, J.G., Keene, W.C., Young, C.J., Pszenny, A. A. P. et al., Roberts, J.M., 2013. Understanding the role of the ground surface in HONO vertical structure: High resolution vertical profiles during NACHTT-11. J. Geophys. Res. Atmos. 118, 10155–10171.

VandenBoer, T.C., Markovic, M.Z., Sanders, J.E., Ren, X., Pusede, S.E., Browne, E.C. et al., 2014. Evidence for a nitrous acid (HONO) reservoir at the ground surface in Bakersfield, CA, during CalNex 2010. J. Geophys. Res. Atmos. 119, 9093-9106.

VandenBoer, T.C., Young, C.J., Talukdar, R.K., Markovic, M.Z., Brown, S.S., Roberts, J.M., Murphy, J.G., 2015. Nocturnal loss and daytime source of nitrous acid through reactive uptake and displacement. Nature Geosci. 8, 55–60.

Veitel, H., 2002. Vertical Profiles of NO_2 and HONO in the Planetary Boundary Layer [WWW Document]. URL http://archiv.ub.uni-heidelberg.de/volltextserver/2490/ (accessed 10.6.15).

Villena, G., Kleffmann, J., Kurtenbach, R., Wiesen, P., Lissi, E., Rubio, M.A. et al., 2011. Vertical gradients of HONO, NOx and O3 in Santiago de Chile. Atmospheric Environment 45, 3867–3873.

Walcek, C.J., Brost, R.A., Chang, J.S., Wesely, M.L., 1986. SO_2, sulfate and HNO_3 deposition velocities computed using regional landuse and meteorological data. Atmospheric Environment 20, 949–964.

Wong, K.W., Tsai, C., Lefer, B., Grossberg, N., Stutz, J., 2013. Modeling of daytime HONO vertical gradients during SHARP 2009. Atmos. Chem. Phys.13, 3587–3601.

Wong, K.W., Tsai, C., Lefer, B., Haman, C., Grossberg, N., Brune, W.H. et al., 2012. Daytime HONO vertical gradients during SHARP 2009 in Houston, TX. Atmos. Chem. Phys. 12, 635–652.

Ye, C., Zhou, X., Pu, D., Stutz, J., Festa, J., Spolaor, M. et al., 2015. Comment on "Missing gas-phase source of HONO inferred from Zeppelin measurements in the troposphere." Science 348, 1326-d.

Young, C.J., Washenfelder, R.A., Roberts, J.M., Mielke, L.H., Osthoff, H.D., Tsai, C. et al., 2012. Vertically resolved measurements of nighttime radical reservoirs in Los Angeles and their contribution to the urban radical budget. Environ. Sci. Technol. 46, 10965–10973.

Zhang, N., Zhou, X., Shepson, P.B., Gao, H., Alaghmand, M., Stirm, B., 2009. Aircraft measurement of HONO vertical profiles over a forested region. Geophys. Res. Lett. 36, L15820.

Zhou, X., Gao, H., He, Y., Huang, G., Bertman, S.B., Civerolo, K., Schwab, J., 2003. Nitric acid photolysis on surfaces in low-NOx environments: Significant atmospheric implications. Geophysical Research Letters 30(23), 2217.

Zhou, X., Zhang, N., TerAvest, M., Tang, D., Hou, J., Bertman, S. et al., 2011. Nitric acid photolysis on forest canopy surface as a source for tropospheric nitrous acid. Nature Geosci. 4, 440–443.

595 Table 1. HONO source and sink mechanisms considered for modeling HONO in the outflow of the DFW metropolitan area.

Mechanism	ID	Parameter	Lower-limit	Likely	Upper-limit	Reference
Aerosol uptake of NO_2	B1	γ_{NO2} (-)	2.0×10^{-7}	1.0×10^{-6}	5.0×10^{-6}	Kleffmann et al. (1998); Aumont et al.(2003)
Photoenhanced aerosol uptake of NO_2	B2	$\gamma_{NO2,hv}$ (-)	4.0×10^{-6}	1.0×10^{-5}	1.0×10^{-3}	Stemmler et al. (2007); Wong et al. (2013)
Photoenhanced conversion of NO_2 soot	B3	$\gamma_{soot,BET}$ (-)	4.0×10^{-7}	5.0×10^{-7}	6.0×10^{-7}	Monge et al. (2010)
		BET surface area (cm^2/g)	9.7×10^{5}	1.2×10^{6}	1.3×10^{6}	
Direct HONO emission	B4	f_{emiss} (%v, $\Delta HONO/\Delta NO_x$)	0.0029	0.0055	0.0080	Kirchstetter et al. (1996); Kurtenbach et al. (2001)
OH + NO	B5	$k\infty$(T) (cm^3 $molec^{-1}$ s^{-1})	3.0×10^{-11}	3.6×10^{-11}	4.3×10^{-11}	NASA (2011)
		k_o(T) (cm^6 $molec^{-2}$ s^{-1})	5.8×10^{-31}	7.0×10^{-31}	8.4×10^{-31}	NASA (2011)
HONO from surface HNO_3 photolysis	B6	$j_{HNO3\text{-}HONO}$ (s^{-1})	1.0×10^{-5}	1.2×10^{-5}	1.4×10^{-5}	Zhou et al. (2003)
		$v_{d,\ HNO3}$ (cm s^{-1})	1.50	1.75	2.25	Walcek et al. (1986)
HONO from NO_2 conversion at ground	B7	$\gamma_{NO2,\ gr}$ (-)	1.0×10^{-6}	5.0×10^{-6}	1.0×10^{-5}	Kleffmann et al. (1998); Kurtenbach et al. (2001)
Photoenhanced NO_2 conversion, ground	B8	$\gamma_{NO2,gr,hv}$ (-)	1.7×10^{-5}	2.0×10^{-5}	6.0×10^{-5}	Stemmler et al. (2006); Wong et al. (2013)
HNO_3 →HONO, VOC	S1	$f_{HNO3,\ VOC}$ (ppt s^{-1})	3.6×10^{-2}	5.8×10^{-2}	8.3×10^{-2}	Rutter et al. (2014)
Biotic release, ground	S2	f_{soil} (molec cm^{-2} s^{-1})	-	1.7×10^{9}	4.0×10^{9}	Oswald et al. (2013)
Re-emission from NO_2-(p) reservoir	S3	$v_d \times \eta$ (cm s^{-1})	1.0×10^{-2}	9.0×10^{-2}	2.0×10^{-1}	Vandenboer et al. (2014)
HONO uptake at ground	L1	$\gamma_{HONO,gr}$ (-)	1.0×10^{-4}	2.0×10^{-5}	1.8×10^{-5}	Vandenboer et al. (2013); Wong et al. (2013); Trick (2004)
HONO + OH	L2	$k_{HONO+OH}$ (cm^3 $molec^{-1}$ s^{-1})	6.75×10^{-12}	4.5×10^{-12}	3.0×10^{-12}	NASA (2011)
HONO photolysis	L3	j_{HONO} (s^{-1})	1.8×10^{-3} - 3.9×10^{-5} [a]			This investigation

596 [a]Maximum-minimum range of the experimentally determined time-series values of j_{HONO} input to the model (not varied).

597 Table 2. Best estimates of parameterizations of sources and sinks of HONO in the outflow of
598 DFW for baseline and scenario GrN S2/S3.

		Best-fit estimate (% difference from 'likely')	
ID	**Parameter**	**GrN S2, S3**	**GrN Baseline**
B1	γ_{NO2} (-)	3.9×10^{-6} (294%)	2.5×10^{-6} (152%)
B2	$\gamma_{NO2,hv}$ (-)	8.5×10^{-4} (8500%)	1.0×10^{-3} (9900%)
B3	$\gamma_{soot,BET}$ (-)	5.3×10^{-7} (6%)	5.3×10^{-7} (7.1%)
	BET surface area (cm^2/g)	1.1×10^{2} (-6.5%)	1.2×10^{2} (-3%)
B4	f_{emiss} (%v, $\Delta HONO/\Delta NO_2$)	0.0043 (-22%)	0.0049 (-10%)
B5	$k\infty$(T) (cm^3 $molec^{-1}$ s^{-1})	3.7×10^{-11} (4.4%)	3.8×10^{-11} (4.8%)
	k_o(T) (cm^6 $molec^{-2}$ s^{-1})	7.6×10^{-31} (9%)	7.3×10^{-31} (4.8%)
B6	$j_{HNO3\text{-}HONO}$ (s^{-1})	1.2×10^{-5} (-3%)	1.3×10^{-5} (7.7%)
	$v_{d,\ HNO3}$ (cm s^{-1})	1.8 (4.6%)	2.0 (17%)
B7	$\gamma_{NO2,\ gr}$ (-)	6.1×10^{-6} (22%)	9.9×10^{-6} (97%)
B8	$\gamma_{NO2,gr,hv}$ (-)	6×10^{-5} (200%)	6×10^{-5} (200%)
S1	$f_{HNO3,\ VOC}$ (ppt s^{-1})	n/a	n/a
S2	f_{soil} (molec cm^{-2} s^{-1})	2.8×10^{9} (66%)	n/a
S3	$v_d \times \eta$ (cm s^{-1})	0.18 (105%)	n/a
L1	$\gamma_{HONO,gr}$ (-)	5.7×10^{-5} (185%)	2.0×10^{-5} (-1.1%)
L2	$k_{HONO+OH}$ (cm^3 $molec^{-1}$ s^{-1})	5.7×10^{-12} (28%)	4.6×10^{-12} (2.1%)
L3	j_{HONO} (s^{-1})	unchanged	unchanged
	Missing source or sink: daytime, nighttime (ppt s^{-1})	0.10, -0.0112	0.15, -0.006

599

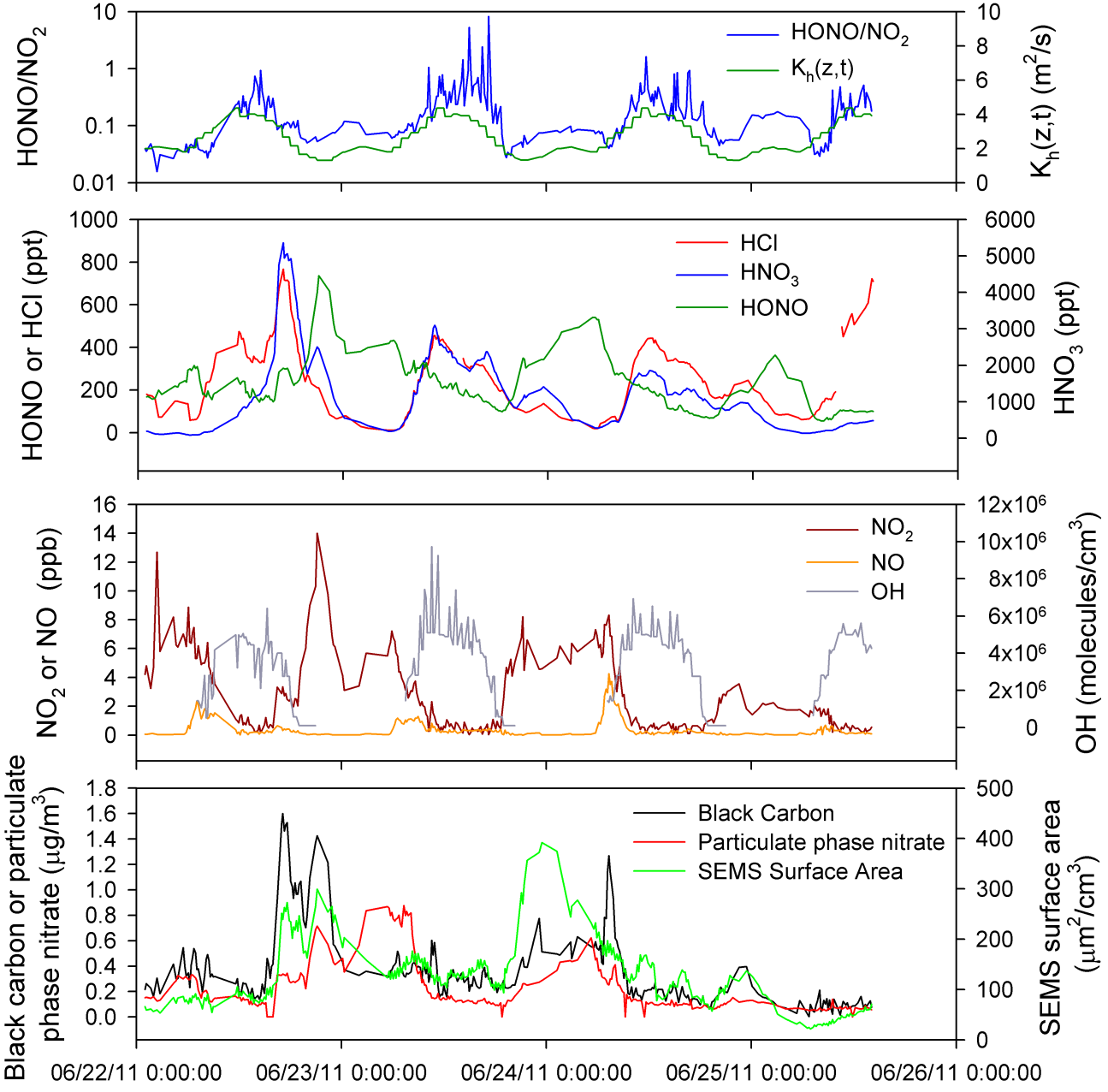

Figure 1. Time series inputs to the two-layer box model of HONO mixing ratios in the outflow of DFW.

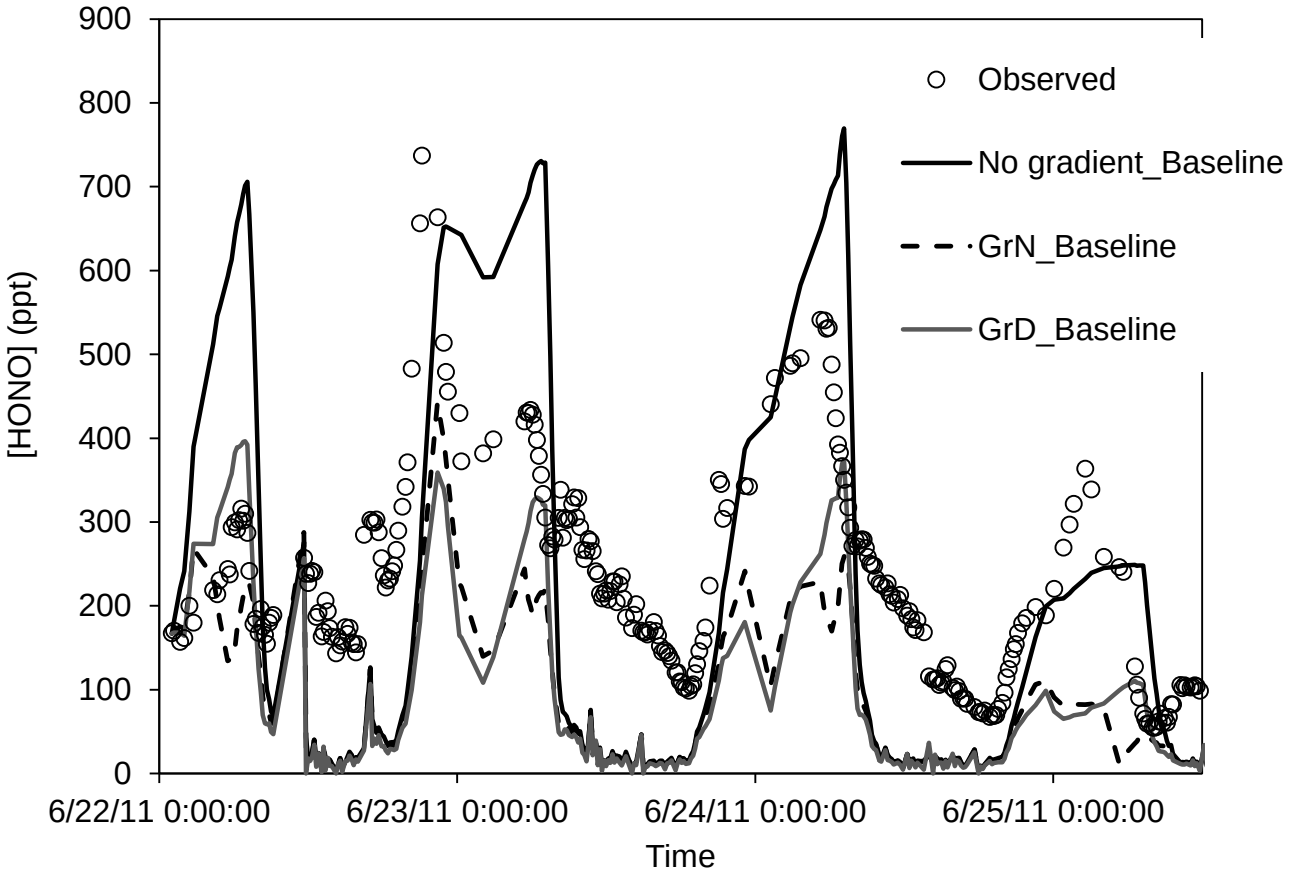

Figure 2. Model output for 'likely' estimates of parameterizations under conditions of no gradient, stronger nighttime gradient (GrN), and stronger daytime gradient (GrD).

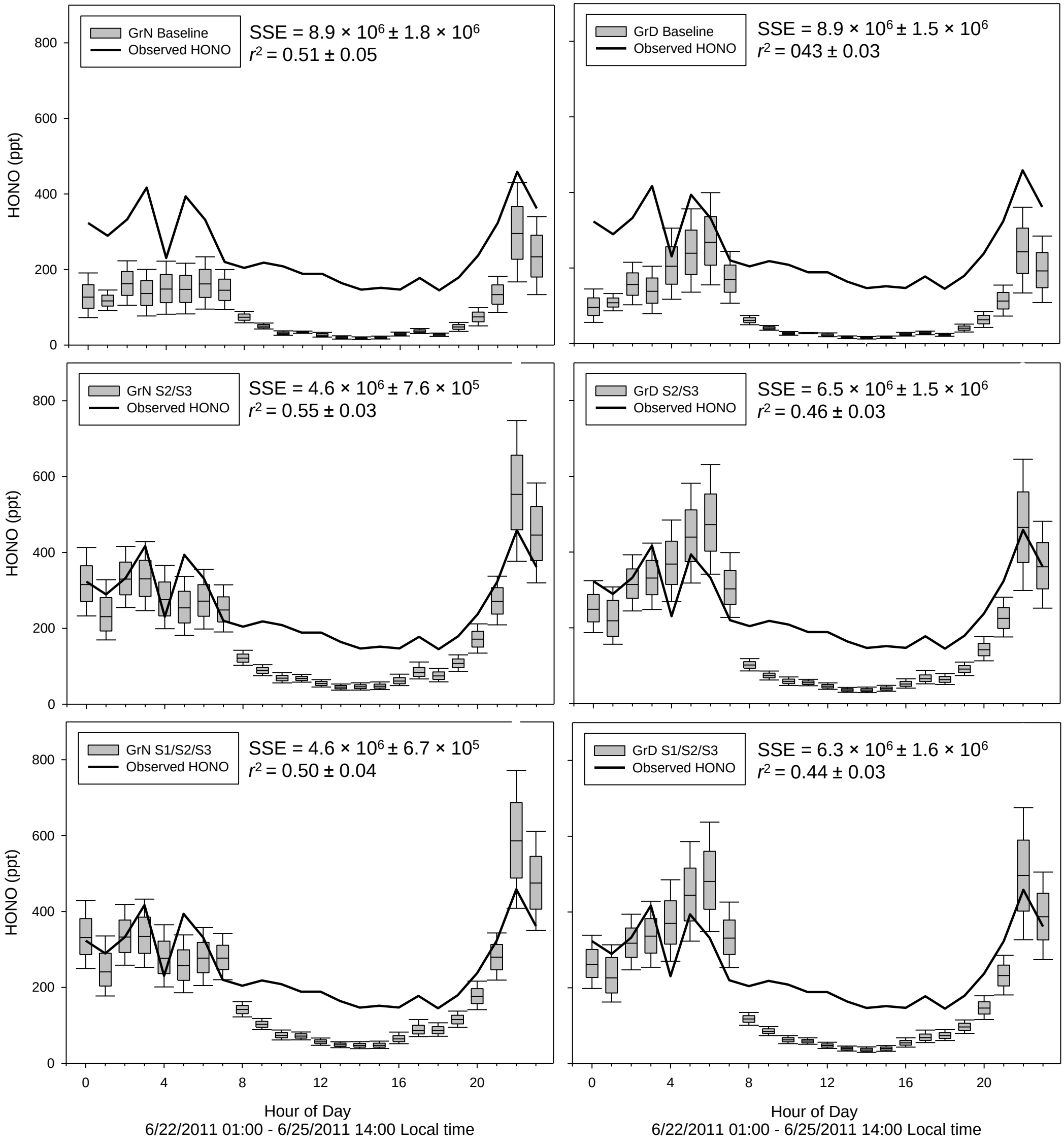

Figure 3. Summary of Monte Carlo simulation output for baseline scenarios, and scenarios with S2/S3 and S1/S2/S3 added to the baseline scenario.

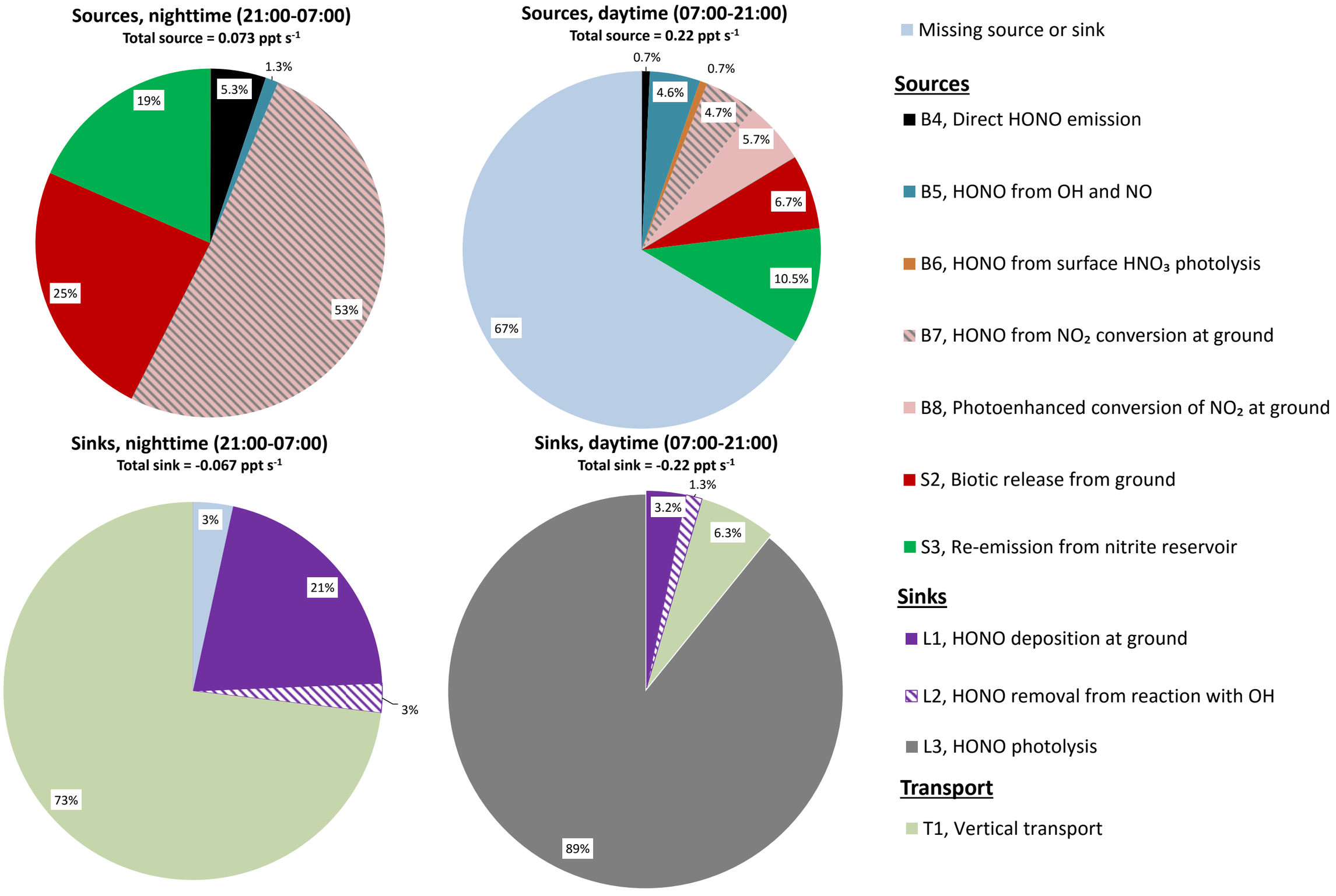

Figure 4. Relative contribution to HONO source or sink strength in GrN S2/S3 with 'likely' estimates of parameterizations. Contributions are averaged for the time period indicated above each pie chart across the modeling period (6/22/2011 01:00 – 6/25/2011 14:00 local time). Unknown source or sink is determined by stepwise addition of HONO source or sink such that modeled HONO equals measured HONO.

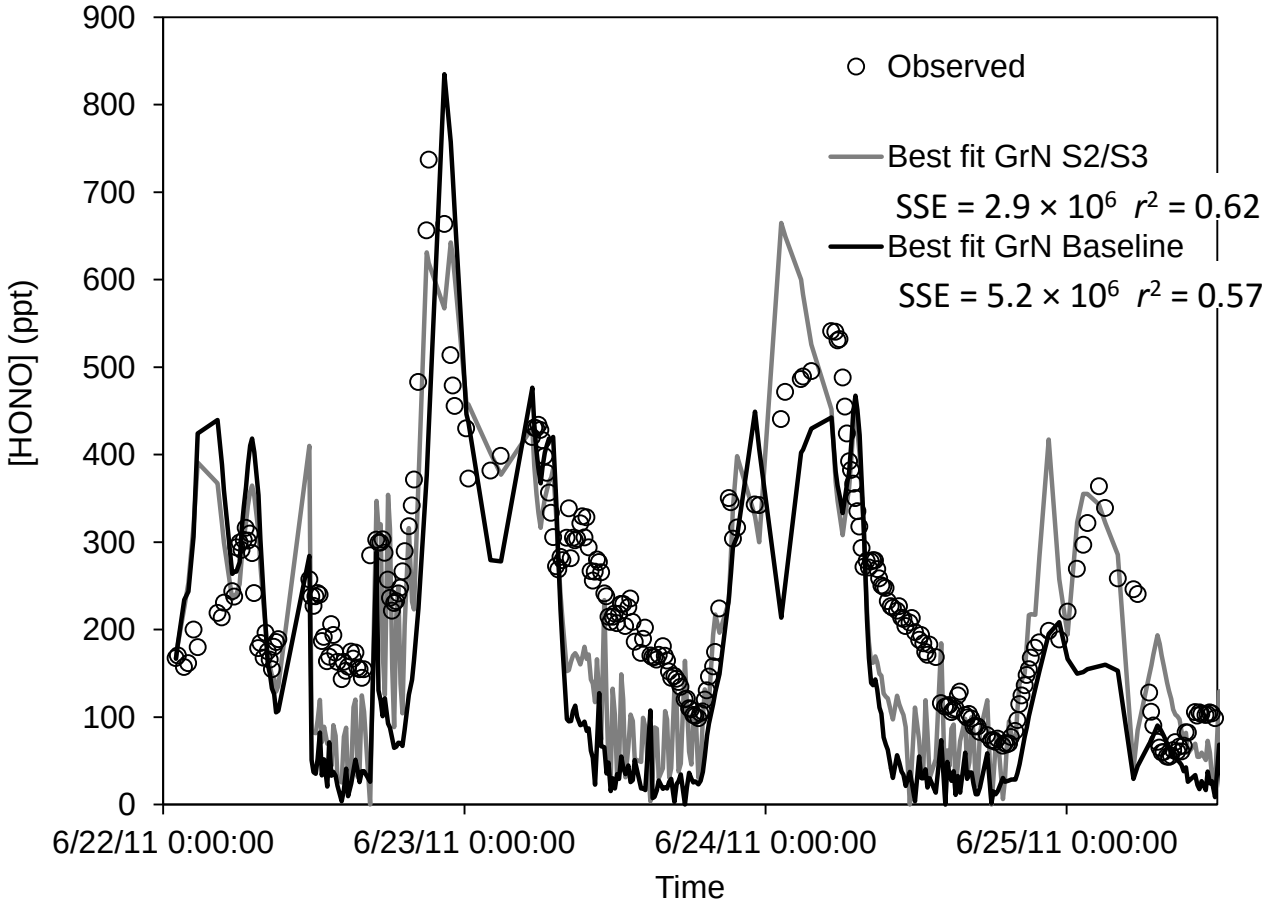

Figure 5. Model performance with best-fit parameters for the nighttime gradient (GrN) scenario with sources S2 and S3, compared to the nighttime gradient scenario with only baseline sources included.

- A two-layer box model evaluates HONO sources, sinks in outflow of Dallas-Fort Worth
- Monte Carlo simulation is applied to scenarios with 3 recently identified sources
- Improved model outcomes result from inclusion of 2 of 3 recently identified sources
- A substantial unknown source is still required for agreement with observation
- Missing HONO source is moderately correlated with j_{NO2}, weakly correlated with NO_2